Photocatalysis Hot Paper

DOI: 10.1002/anie.201311280

Monolayer HNb_3O_8 for Selective Photocatalytic Oxidation of Benzylic Alcohols with Visible Light Response**

Shijing Liang, Linrui Wen, Sen Lin, Jinhong Bi, Pingyun Feng, Xianzhi Fu, and Ling Wu**

Abstract: *Monolayer HNb_3O_8 2D nanosheets have been used as highly chemoselective and active photocatalysts for the selective oxidation of alcohols. The nanosheets exhibit improved photocatalytic activity over their layered counterparts. Results of in situ FTIR, DRS, ESR, and DFT calculations show the formation of surface complexes between the Lewis acid sites on HNb_3O_8 2D nanosheets and alcohols. These complexes play a key role in the photocatalytic activity of the material. Furthermore, the unique structural features of the nanosheets contributed to their high photocatalytic activity. An electron transition from the coordinated alcohol species to surface Nb atoms takes place and initiates the aerobic oxidation of alcohols with high product selectivity under visible light irradiation. This reaction process is distinct from that of classic semiconductor photocatalysis.*

Heterogeneous photocatalysis has been considered as a promising process for environmental purification, clean energy production, and fine chemical synthesis.[1] Over the past decades, extensive efforts have been devoted to the development of highly efficient and active photocatalysts.[2] However, a significant open issue is that a thorough understanding of the catalytic mechanism has not yet been achieved. The understanding of photocatalytic chemistry on a molecular level is desirable, and would shed light on the rational design, synthesis, and more effective application of photocatalysts. Anpo et al. attempted to elucidate intrinsic photocatalysis through the development of single-site photocatalysts,[3] which unfortunately contain a low content of active sites and therefore exhibit poor activity. It is necessary to develop new optimal photocatalysts based on new concepts.

Recently, two dimensional (2D) oxide nanosheets have sparked worldwide interest because of the novel electronic structures, distinctive physicochemical properties, and their functionalities inherited from the layered parent compounds.[4] These nanosheets crystallites could show exceptionally high 2D anisotropy: a molecular thickness of 0.5–3 nm versus several hundred nanometers or more in lateral size. The 2D configuration can provide an extremely high percentage of exposed specific crystal facet, huge specific surface area, and large fraction of unsaturated surface metal sites (USMSs).[5] The USMSs could function as active sites and contact with the substrate intimately. And thus, it is highly desirable to fabricate suitable metal oxide 2D nanosheets in efforts to achieve efficient photocatalytic reaction.[6] Undoubtedly, the introduction of 2D nanosheets for photocatalysis not only widens the application of the nanosheets themselves, but may also provide unprecedented opportunities for a deep understanding of the interaction between the active sites and the reactants.

Herein, we employ HNb_3O_8 2D nanosheets of molecular thickness as a high chemoselective and active material for the photocatalytic selective oxidation of benzylic alcohols to the corresponding aldehydes using oxygen as oxidant under visible light irradiation for the first time. It was revealed that formation of the surface complexes in situ between the USMS and the organic reactant species contributed to harvesting visible light and induced the photocatalytic reaction. The coordination structures were characterized by various advanced molecular spectroscopic techniques and DFT calculations. Finally, a reaction mechanism distinctly different from the classic photocatalytic reaction process has been proposed on the basis of detailed experimental results.

HNb_3O_8 2D nanosheets were prepared by a cation-exchange/exfoliation process using layered KNb_3O_8 as a precursor. The detailed preparation procedure is described in the Supporting Information (Experimental section and Figure S1). As shown in Figure S2, the X-ray diffraction peaks of the layered KNb_3O_8 and HNb_3O_8 match well with the published data (JCPDS: 75-2182 and 44-0672, respectively). The characteristic (020) peak shifted to a lower 2θ angle after the proton-exchange process, indicating that the interlayer distance of HNb_3O_8 ($d = 1.12$ nm) is wider than that of KNb_3O_8 ($d = 1.06$ nm). This will benefit the intercalation of tetrabutylammonium (TBA) cations in a subsequent cation-exchange process. Compared with the layered parent compounds, HNb_3O_8 nanosheets obtained by exfoliation just exhibit two very weak and broad diffraction peaks. These reveal the loss of the periodic layered structure of HNb_3O_8, as well as long-range ordering in the HNb_3O_8 nanosheet materials.[7] This could serve as strong evidence for the existence of HNb_3O_8 nanosheets with single layer.

[*] Dr. S. Liang, L. Wen, Dr. S. Lin, Dr. J. Bi, Prof. X. Fu, Prof. L. Wu
State Key Laboratory of Photocatalysis on Energy and Environment, Fuzhou University, Fuzhou 350002 (P.R. China)
E-mail: wuling@fzu.edu.cn
Prof. P. Feng, Prof. L. Wu
Department of Chemistry, University of California
Riverside, CA 92521 (USA)
E-mail: pingyun.feng@ucr.edu

[**] This work was supported by the National Natural Science Foundation of China (21303019, 21177024, 21203026, 21003022, and 21273036), National Science Foundation (CHE-1213795, P.F.), Natural Science Foundation of Fujian Province (2011J01041), and National Key Basic Research Program of China (973 Program: 2014CB239303).

Supporting information for this article is available on the WWW under http://dx.doi.org/10.1002/anie.201311280.

SEM images show KNb_3O_8 and HNb_3O_8 contain a typical layer structure stacked layer by layer (Figure S3 a,b). The thickness of layered HNb_3O_8 flakes is about 50 nm. In contrast, our HNb_3O_8 material is mainly composed of rather loose and irregular tissue-like 2D nanosheets. This morphology is also confirmed by the TEM image (Figure 1 a). The nanosheets, with a lateral scale ranging from submicrometer to several micrometers, are nearly transparent, indicating they are ultrathin. A Tyndall effect in the suspension (Figure 1 A, insert) reveals the presence of highly monodisperse ultrathin HNb_3O_8 nanosheets in water. The selected-area electron diffraction (SAED) pattern (Figure 1 B) shows the single-crystalline characteristics of HNb_3O_8 nanosheets. The clear lattice image and sharp electron diffraction pattern demonstrate that nanosheets retain the high crystallinity, which is reconfirmed by the HRTEM image (Figure 1 C). The angle labeled in the SAED pattern is 90°, which is in agreement with the theoretical value of the angle between the (001) and (100) planes. The set of diffraction spots can be indexed as the [010] zone axis of HNb_3O_8; that is, the bottom and top surfaces of the HNb_3O_8 nanosheets are {010} facets, and the percentage of exposed {010} facets is over 99 %. Atomic force microscopy (AFM) images show that the as-prepared sample has a 2D nanosheet structure and a smooth surface (Figure 1 D). The typical thickness of the HNb_3O_8 nanosheets is about 1.1 nm, which agrees well with the 1.05 nm of a single-layered HNb_3O_8 slab along the [010] direction, providing direct and solid evidence for the formation of monolayer HNb_3O_8 of molecular thickness. This monolayer induces an increase of the surface disorder of single-layer HNb_3O_8.[6c,8] The electronic properties of HNb_3O_8 nanosheets would be inevitably influenced, resulting in higher carrier conductivity and mobility.

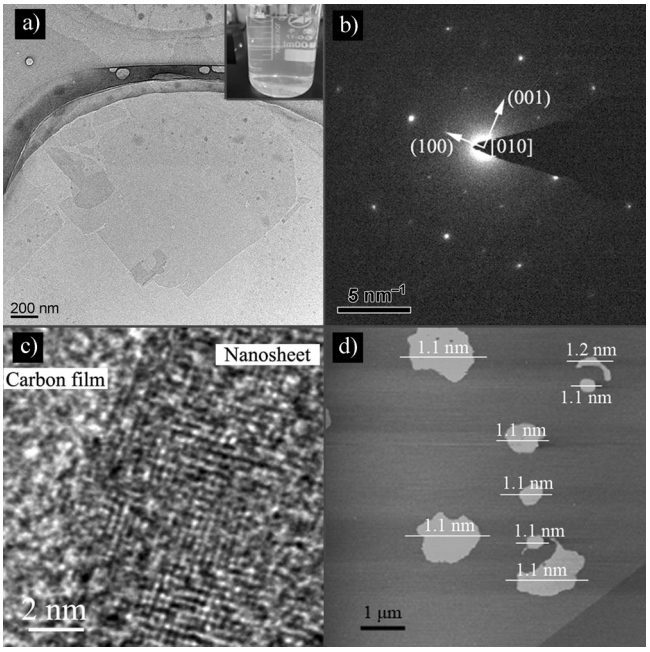

Figure 1. TEM (a), SAED pattern (b), HRTEM (c), and AFM (d) images of HNb_3O_8 nanosheet. The inset in (a) shows the Tyndall effect of HNb_3O_8 nanosheets dispersed in water.

The BET surface area of the HNb_3O_8 nanosheets is about 86.7 $m^2 g^{-1}$, which is 45 times larger than that of layered HNb_3O_8 (1.9 $m^2 g^{-1}$). The adsorption–desorption isotherm of nanosheets is a type IV isotherm, whereas the layered HNb_3O_8 displays a type II isotherm (Figure S4 a). The pore-size distribution of HNb_3O_8 nanosheets mainly ranges from 2.5 to 40 nm (Figure S4 b), suggesting that the as-exfoliated HNb_3O_8 maintains the free-standing nanosheet form, and is not a layered compound after precipitation.

The aerobic oxidations of benzylic alcohols were carried out as the test reactions (Table 1). Under visible light irradiation and controlled temperature at 298 K, HNb_3O_8 nanosheets shows high activity, chemoselectivity, and versatility for the aerobic oxidation of alcohols (Table 1, entries 1–5). For example, the conversion of 4-methylbenzyl alcohol (4-MBA) reaches 54 % with an extremely high selectivity (> 99 %), which is about 36 times higher than that of the layered parent HNb_3O_8 (Table 1, entry 6). There was no obvious loss in terms of the catalytic activity during five consecutive runs (Figure S5). After the reaction, HNb_3O_8 nanosheets could be easily separated and reused. Interestingly, *para*-substituted benzyl alcohols containing electron-donating groups (such as CH_3 and OCH_3; Table 1, entries 1–2) are more easily oxidized than those containing electron-withdrawing groups (such as F and Cl; Table 1, entries 4–5). In the latter case, the reaction rate is comparable to that of unsubstituted benzyl alcohol (BA). These suggest that the reaction may proceed through the intermediacy of a carbocationic species.[9] It is worth noting that the nanosheets exhibit much higher photocatalytic activity than most of the reported photocatalysts (Table S2). As comparison, the layered parent HNb_3O_8 shows very low conversion rates for all *para*-substituted benzylic alcohols (Table S1, entries 1–5). For the oxidation of BA over layered HNb_3O_8, only trace of benzaldehyde was been detected. Therefore, this greatly improved photocatalytic activity may originate from the unique structure features of 2D nanosheets, such as molecular thickness, large surface area, and more active sites.

Table 1: Photocatalytic activity for the selective oxidation of benzylic alcohols over HNb_3O_8 nanosheets with visible light irradiation.

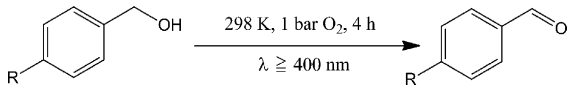

Entry	Cat.	R	Atm.	Conversion [%]	Selectivity [%]
1	NN	OCH_3	O_2	63	85
2	NN	CH_3	O_2	54	> 99
3	NN	H	O_2	20	> 99
4	NN	Cl	O_2	28	> 99
5	NN	F	O_2	18	> 99
6	LN	CH_3	O_2	1.5	> 99
7[a]	–	CH_3	O_2	0	–
8	NN	CH_3	air	17	> 99
9	NN	CH_3	N_2	2	> 99

[a] Photolysis of 4-methylbenzyl alcohol. LN = layered HNb_3O_8, NN = HNb_3O_8 nanosheets.

Furthermore, a set of control experiments were carried out to confirm the photocatalytic process. As shown in Table 1, entry 7, the transformation of 4-MBA can be negligible in absence of catalysts under visible light irradiation. Additionally, the thermocatalysis of HNb_3O_8 nanosheets toward selective oxidation of 4-MBA can also be negligible at 298–353 K (Table S1, entries 6–8). A dramatic decrease in catalytic activity when the reaction was carried out in air, and a near inactivation in a N_2 atmosphere indicate that both O_2 and the HNb_3O_8 nanosheets are necessary for the oxidation of benzylic alcohols (Table 1, entries 8–9).

Brønsted and Lewis acid sites on HNb_3O_8 nanosheets and layered HNb_3O_8 were investigated in situ by FTIR spectroscopy (Figure 2a,b). As shown in Figure 2a, two strong peaks

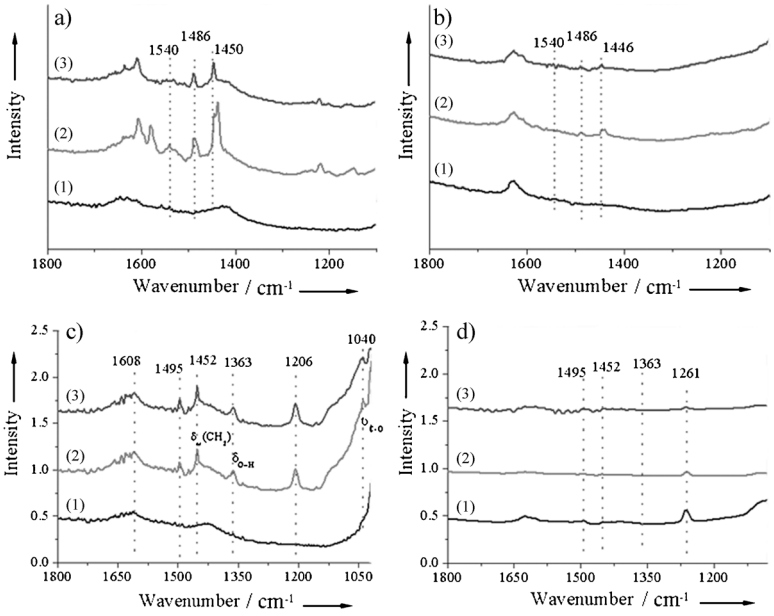

Figure 2. In situ FTIR spectra of the HNb_3O_8 nanosheets (a,c) and layered HNb_3O_8 (b,d) disks before and after adsorbed pyridine (a,b) and benzyl alcohol (c,d). Conditions: (1) After degassing at 300°C for 2 h. (2) Adsorption for 30 min at RT (physisorption + chemisorption). (3) Further evacuation of excess probe molecules at 150°C for 3 min under 6×10^{-4} Torr (chemisorption).

at 1450 and 1486 cm^{-1} on the HNb_3O_8 nanosheets can be assigned to pyridine on the Lewis acid and Brønsted acid sites, respectively.[10] These peaks also remained even after evacuation. It is suggested that the Lewis acid sites are derived from the unsaturated surface Nb atoms (Figure S6). Furthermore, a broad and weak peak at 1540 cm^{-1}, which is attributed to pyridine on the Brønsted acid sites, was also observed.[10] In contrast, these peaks on layered HNb_3O_8 are much weaker (Figure 2b). It can also be seen that the amount of acid in HNb_3O_8 nanosheets is much higher than that of layered HNb_3O_8, which can be further verified by ^1H NMR spectroscopy (Figure S7). The surface acidity of the catalyst plays a very important role in the selective photocatalytic organic transformation (SPOT) reaction. Brønsted acids can dramatically promote the reaction rate of oxidation of alcohols,[11] and Lewis acidic sites may act as the reactive site.[12] Therefore, the strong Brønsted and Lewis acidity contribute to the high photocatalytic activity of the HNb_3O_8 nanosheets.

As HNb_3O_8 and alcohols would not have visible light activity (Figure S8), considering that the alcohols could be adsorbed on the Lewis acid sites by Lewis acid–base interaction, we propose that the formation of surface complexes could be responsible for the active site, and thus promote the response of the SPOTs under visible light irradiation. This has also been witnessed in previous reports over bulk Nb_2O_5 and TiO_2.[12,13] After BA is adsorbed, the samples show considerable visible light absorption (Figure S8c,d). Furthermore, samples adsorbed with ethanol or benzene do not exhibit absorption in the visible light region (Figure S9). It could, therefore, be assumed that this absorption in the visible light region was assigned to the ligand-to-metal charge transfer (LMCT) of the surface complex.[13a] The in situ FTIR spectra of BA/HNb_3O_8 (Figure 2c,d) show the chemisorption of abundant BA on the surface of HNb_3O_8, thus indicating the formation of a surface complex. ESR spectra also show the clear decrease of the concentration of unsaturated Nb atoms and the existence of BA species (Figure S10c), thus confirming the formation of a surface complex. Remarkably, the characteristic O–H and C–O band of BA is shifted to a lower wavenumber after being adsorbed on the surface of the HNb_3O_8 nanosheet, whereas the other characteristic bands of BA show no change compared with those of free BA (Figure S11). These results suggest the formation of a surface complex by a -C-O-Nb- coordinate bond.

To understand the interaction between BA and the HNb_3O_8 nanosheets, we carried out ab initio density-functional theory (DFT) calculations (Figures S12–14). The results show that the most stable adsorption configuration of BA is the simultaneous formation of a -C-O-Nb- coordinate bond and an -O-H-O′- hydrogen bond (where the O atom is from benzyl alcohol and the O′ atom is the crystal lattice oxygen of a HNb_3O_8 nanosheet). This adsorption energy is estimated at about −1.67 eV. In comparison, the adsorption energy of BA is about −0.49 eV in the absence of a -C-O-Nb- coordinate bond. From Figure S14, a coupling between the p orbital of the hydroxy O atom and the d orbital of the Nb atom below the Fermi energy level can be found after the local density of states (LDOS) analysis. These results reveal the formation of a surface complex through -C-O-Nb- coordinate bonds.

Notably, the concentration of BA adsorbed on HNb_3O_8 nanosheets is much higher than that on layered HNb_3O_8. As a result, the BA/HNb_3O_8 nanosheets exhibit much stronger absorption of visible light compared with BA/layered HNb_3O_8. This is due to the fact that the concentration of unsaturated surface Nb atoms on HNb_3O_8 nanosheets is much higher than that of layered HNb_3O_8, which can be demonstrated by the results of DRS[14] and EPR spectra (Fig-

ure S10a,b). One can also see different colors in the HNb_3O_8 samples before and after BA is grafted.

In an attempt to gain some insight into the reaction mechanism, we conducted EPR measurements for BA adsorbed on HNb_3O_8 nanosheets and layered HNb_3O_8 under an O_2 atmosphere at 77 K (Figure S15–16). A tiny EPR signal around $g = 2.003$, which was assigned to an oxygen vacancy, and a set of signals assigned to the benzyl alcohol radical are observed when the reaction was conducted in the dark (Figure S15a,c). Under visible light irradiation, an intense signal consisting of one set of rhombic g values ($g_1 = 2.036$, $g_2 = 2.003$, $g_3 = 1.986$) is observed (Figure S15d). These signals are attributed to $\cdot O_2^-$, which derives from the reduction of adsorbed O_2 by excited electrons.[15] Furthermore, the signals of benzyl alcohol radicals are also enhanced. These results suggest that O_2 is adsorbed on an uncoordinated Nb atom near the surface complex. As comparison, no signal has been observed over BA/layered HNb_3O_8 both with and without visible light irradiation (Figure S16). This may be due to the poor concentration of the surface complex formed in situ. Moreover, we also detect the formation of hydrogen peroxide in the reaction process (Figure S17).

On the basis of the results of the aforementioned experiments, a tentative mechanism is proposed as depicted in Scheme 1: 1) Alcohol and O_2 are competitively adsorbed on

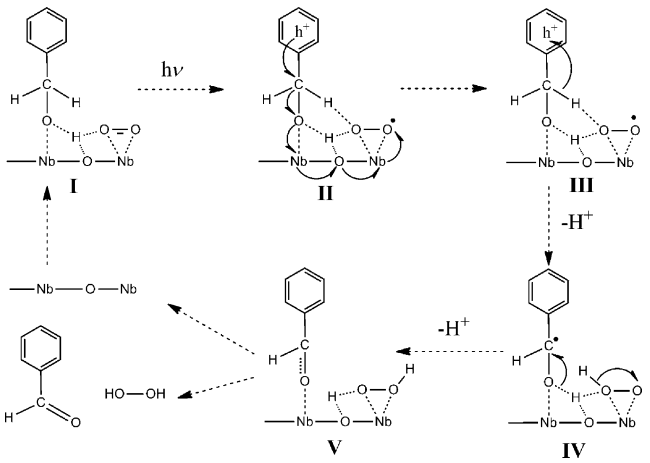

Scheme 1. Reaction mechanism of alcohol photooxidation over HNb_3O_8 nanosheets with molecular oxygen.

HNb_3O_8 nanosheets in the dark (**I**). 2) Under visible light irradiation, a ligand-to-metal charge transfer (LMCT) of the surface complex would take place; the adsorbed O_2 would be simultaneously reduced to superoxide ($\cdot O_2^-$) (**II**). 3) Subsequently, the photogenerated hole would induce the α-deprotonation from BA with assistance from the superoxide radical (**III**). 4) The superoxide species would further induce deprotonation from the complex to form the corresponding aldehyde and hydrogen peroxide (**IV** and **V**). 5) Finally, the aldehyde and H_2O_2 molecules are released from the nanosheet surface and the regeneration of the uncoordinated surface Nb sites of the HNb_3O_8 nanosheet completes the photocatalytic oxidation cycle. The formed H_2O_2 could also be transformed into H_2O by a series of reactions. This is distinct from the mechanism of classic semiconductor photocatalysis, which is initiated by the formation of a photogenerated electron in the conduction band of the semiconductor and a positive hole in its valence band.

To generalize this concept, we also developed other metal oxide 2D nanosheets for selective oxidation of alcohols and amines (Such as $Ti_{0.87}O_2$, $H_3Ti_5NbO_{14}$, and $HTaO_3$ nanosheets). All of these nanosheets show a greatly enhanced activity for SPOTs compared with their layered counterparts (Table S3). It is believed that the use of 2D nanosheets and their activation by surface complexes will be a powerful approach to bestow these SPOTs with high chemoselectivity and activity.

In conclusion, we have introduced HNb_3O_8 nanosheets as highly chemoselective and active photocatalysts for the selective oxidation of alcohols by oxygen. It takes place through a different photoactivation mechanism from the classical mechanism in photocatalysis. The formation of a surface complex, acting as the reactive center, is the key to achieve the SPOTs high activity. Due to the features of 2D nanosheets, such as molecular thickness, large surface area, abundant Lewis acid sites, strong Brønsted acidity, and a high concentration of surface complexes, HNb_3O_8 nanosheets exhibit an significantly improved photocatalytic activity for the oxidation of alcohols without loss of selectivity versus its layered parent HNb_3O_8. We believe that the present study will stimulate intensive research in the realization of inherent heterogeneous photocatalysis on a molecular level.

Received: December 30, 2013
Published online: February 12, 2014

Keywords: charge transfer · chemisorption · monolayers · photocatalysis · visible light

[1] a) G. Palmisano, V. Augugliaro, M. Pagliaro, L. Palmisano, *Chem. Commun.* **2007**, 3425–3437; b) T. Ochiai, A. Fujishima, *J. Photochem. Photobiol. C* **2012**, *13*, 247–262; c) Y. Qu, X. Duan, *Chem. Soc. Rev.* **2013**, *42*, 2568–2580; d) S. N. Habisreutinger, L. Schmidt-Mende, J. K. Stolarczyk, *Angew. Chem.* **2013**, *125*, 7516–7557; *Angew. Chem. Int. Ed.* **2013**, *52*, 7372–7408.

[2] a) H. Tong, S. Ouyang, Y. Bi, N. Umezawa, M. Oshikiri, J. Ye, *Adv. Mater.* **2012**, *24*, 229–251; b) A. Kubacka, M. Fernández-García, G. Colón, *Chem. Rev.* **2012**, *112*, 1555–1614.

[3] a) M. Anpo, M. Takeuchi, *J. Catal.* **2003**, *216*, 505–516; b) M. Anpo, J. M. Thomas, *Chem. Commun.* **2006**, 3273–3278; c) Y. Horiuchi, H. Yamashita, *Appl. Catal. A* **2011**, *400*, 1–8.

[4] a) J. N. Coleman, et al., *Science* **2011**, *331*, 568–571, see the Supporting information; b) R. Mas-Ballesté, C. Gómez-Navarro, J. Gómez-Herrero, F. Zamora, *Nanoscale* **2011**, *3*, 20–30; c) G. Pacchioni, *Chem. Eur. J.* **2012**, *18*, 10144–10158; d) Q. H. Wang, K. Kalantar-Zadeh, A. Kis, J. N. Coleman, M. S. Strano, *Nat. Nanotechnol.* **2012**, *7*, 699–712; e) M. Osada, T. Sasaki, *Adv. Mater.* **2012**, *24*, 210–228; f) M. Chhowalla, H. S. Shin, G. Eda, L.-J. Li, K. P. Loh, H. Zhang, *Nat. Chem.* **2013**, *5*, 263–275; g) S. Z. Butler, et al., *ACS Nano* **2013**, *7*, 2898–2926, see the Supporting information; h) K. J. Koski, Y. Cui, *ACS Nano* **2013**, *7*, 3739–3743.

[5] M. A. Bizeto, A. L. Shiguihara, V. R. L. Constantino, *J. Mater. Chem.* **2009**, *19*, 2512–2525.

[6] a) Y. Okamoto, S. Ida, J. Hyodo, H. Hagiwara, T. Ishihara, *J. Am. Chem. Soc.* **2011**, *133*, 18034 – 18037; b) S. Sarina, H. Zhu, Z. Zheng, S. Bottle, J. Chang, X. Ke, J. Zhao, Y. Huang, A. Sutrisno, M. Willans, G. Li, *Chem. Sci.* **2012**, *3*, 2138 – 2146; c) Y. Sun, H. Cheng, S. Gao, Z. Sun, Q. Liu, Q. Liu, F. Lei, T. Yao, J. He, S. Wei, Y. Xie, *Angew. Chem.* **2012**, *124*, 8857 – 8861; *Angew. Chem. Int. Ed.* **2012**, *51*, 8727 – 8731; d) S. Liang, R. Liang, L. Wen, R. Yuan, L. Wu, X. Fu, *Appl. Catal. B* **2012**, *125*, 103 – 110; e) S. Liang, S. Zhu, Y. Chen, W. Wu, X. Wang, L. Wu, *J. Mater. Chem.* **2012**, *22*, 2670 – 2678; f) S. Ida, Y. Okamoto, M. Matsuka, H. Hagiwara, T. Ishihara, *J. Am. Chem. Soc.* **2012**, *134*, 15773 – 15782; g) S. Yang, Y. Gong, J. Zhang, L. Zhan, L. Ma, Z. Fang, R. Vajtai, X. Wang, P. M. Ajayan, *Adv. Mater.* **2013**, *25*, 2452 – 2456.

[7] Z. Zhai, Y. Huang, L. Xu, X. Yang, C. Hu, L. Zhang, Y. Fan, W. Hou, *Nano Res.* **2011**, *4*, 635 – 647.

[8] Y. Sun, Z. Sun, S. Gao, H. Cheng, Q. Liu, J. Piao, T. Yao, C. Wu, S. Hu, S. Wei, Y. Xie, *Nat. Commun.* **2012**, *3*, 1057.

[9] H. C. Brown, Y. Okamoto, *J. Am. Chem. Soc.* **1958**, *80*, 4979 – 4987.

[10] K. Nakajima, Y. Baba, R. Noma, M. Kitano, J. N. Kondo, S. Hayashi, M. Hara, *J. Am. Chem. Soc.* **2011**, *133*, 4224 – 4227.

[11] Q. Wang, M. Zhang, C. Chen, W. Ma, J. Zhao, *Angew. Chem.* **2010**, *122*, 8148 – 8151; *Angew. Chem. Int. Ed.* **2010**, *49*, 7976 – 7979.

[12] T. Shishido, K. Teramura, T. Tanaka, *Catal. Sci. Technol.* **2011**, *1*, 541 – 551.

[13] a) S. Higashimoto, N. Suetsugu, M. Azuma, H. Ohue, Y. Sakata, *J. Catal.* **2010**, *274*, 76 – 83; b) X. Lang, W. Ma, Y. Zhao, C. Chen, H. Ji, J. Zhao, *Chem. Eur. J.* **2012**, *18*, 2624 – 2631.

[14] R. Brayner, F. Bozon-Verduraz, *Phys. Chem. Chem. Phys.* **2003**, *5*, 1457 – 1466.

[15] S. Furukawa, T. Shishido, K. Teramura, T. Tanaka, *J. Phys. Chem. C* **2011**, *115*, 19320 – 19327.

